Impacts of Changes in Precipitation Amount and Distribution on Water Resources Studied Using a Model Rainwater Harvesting System

Behzad Asadieh and Nir Y. Krakauer

Ph.D. Candidate (**Asadieh**) and Associate Professor (**Krakauer**), Civil Engineering Department and NOAA-CREST, The City College of New York, City University of New York, 160 Convent Avenue, New York, NY 10031 (E-Mail/Asadieh: basadie00@citymail.cuny.edu).

ABSTRACT: Water supply reliability is expected to be affected by both precipitation amount and distribution changes under recent and future climate change. We compare historical (1951-2010) changes in annual-mean and annual-maximum daily precipitation in the global set of station observations from GHCN and climate models from the Inter-Sectoral Impact Model Intercomparison Project (ISI-MIP), and develop the study to 2011-2099 for model projections under high radiative forcing scenario (RCP8.5). We develop a simple rainwater harvesting system (RWHS) model and drive it with observational and modeled precipitation. We study the changes in mean and maximum precipitation along with changes in the reliability of the model

RHWS as tools to assess the impact of changes in precipitation amount and distribution on reliability of precipitation-fed water supplies. Results show faster increase in observed maximum precipitation (10.14% per K global warming) than mean precipitation (7.64% per K), and increased reliability of the model RWHS driven by observed precipitation by an average of 0.2% per decade. The ISI-MIP models show even faster increase in maximum precipitation compared to mean precipitation. However, they imply decreases in mean reliability, for an average 0.15% per decade. Compared to observations, climate models underestimate the increasing trends in mean and maximum precipitation and show the opposite direction of change in reliability of a model water supply system.

(**Key Terms:** Climate Change, Mean and Maximum Precipitation, Precipitation Distribution Change, Water Resources Reliability, Rainwater Harvesting Systems, Climate Models, Observations.)

Introduction

The Fifth Assessment Report of Inter-Governmental Panel on Climate Change (IPCC) indicates that globally, near-surface air temperature increased by approximately 0.78°C, over the 20th century, with greater trend slope in recent decades (Stocker *et al.*, 2013). Anthropogenic climate change is expected to change the distribution, frequency and intensity of precipitation and result in increased intensity and frequency of floods and droughts, with damaging effects on environment and society (Dankers *et al.*, 2013; Field, 2012; Karl *et al.*, 2009; Min *et al.*, 2011; O'Gorman and Schneider, 2009; Solomon *et al.*, 2007; Trenberth, 2011; Trenberth *et al.*, 2003). As a result of global warming, climate models and satellite observations both indicate that atmospheric water vapor content has increased at a rate of approximately 7% per K warming (Allen and Ingram, 2002; Held and Soden, 2006; Trenberth *et al.*, 2005; Wentz *et al.*, 2007), as expected from the Clausius-Clapeyron equation under stable relative humidity (Held and Soden, 2006; Pall *et al.*, 2006). Although change in global-mean precipitation with respect to warming does not scale with the Clausius-Clapeyron equation, and from energy balance considerations the rate of increase might be expected to be around 2% K^{-1} (Held and Soden, 2006; Wu *et al.*, 2013), impact of global warming on extreme precipitation is expected to be stronger (Pall *et al.*, 2006): increasing availability of moisture in the atmosphere can be expected to result in increased

intensity of extreme precipitation (Allan and Soden, 2008; Allen and Ingram, 2002; Asadieh and Krakauer, 2015; O'Gorman and Schneider, 2009; Trenberth, 2011; Trenberth *et al.*, 2003), with proportionally greater impact than for mean precipitation (Lambert *et al.*, 2008; Pall *et al.*, 2006).

Analysis of station observations shows that extreme (annual-maximum daily) precipitation has increased by 10% per K of global warming over 1901 to 2010, which is even larger than the 7% K^{-1} slope of the Clausius-Clapeyron equation (Asadieh and Krakauer, 2015). Faster increase in extreme precipitation than mean precipitation implies a change in precipitation distribution, where the climate shifts to fewer rainy days and more intense precipitation. Changes in precipitation distribution can result in increased intensity and frequency of flood and drought events (Karl *et al.*, 2009; Ricko *et al.*, 2016) and also can affect the availability of fresh water resources (Karl *et al.*, 2009; Li *et al.*, 2013; Liu and Allan, 2013; Oki and Kanae, 2006; Polson *et al.*, 2013; Schewe *et al.*, 2013). Such changes in precipitation distribution could affect the capability of rainwater-fed tanks and reservoirs to capture excessive precipitation and surface run-off (Arnell, 2004; Asadieh and Krakauer, 2015; Hanson and Vogel, 2014; Kumar and Lawrence, 2014; Su *et al.*, 2009), requiring consideration of both precipitation amount and distribution changes in order to design reliable water supply systems (Asadieh and Krakauer, 2015). Climate change impacts on water resources have been widely noted as a concern (Arnell, 2004; Brekke *et al.*, 2009; Oki and Kanae, 2006; Stocker *et al.*, 2013; Vörösmarty *et al.*, 2000). Climate change may increase water stress in regions that experience decreased precipitation and run-off. Even regions with increased average precipitation and run-off may face increased stress on water resources if precipitation distributions change and the excess water is concentrated in already wet periods and seasons (Arnell, 2004; Oki and Kanae, 2006). Thus, change in the seasonality of precipitation as well as its annual total may affect the performance of reservoirs in terms of water supply and flood control (Payne *et al.*, 2004). Global (Arnell, 2004; Kumar and Lawrence, 2014; Oki and Kanae, 2006) as well as regional (Brekke *et al.*, 2004; Fowler *et al.*, 2003; Raje and Mujumdar, 2010; Vicuna *et al.*, 2007) studies have investigated the changes in reliability of water supply systems due to changes in climate and precipitation pattern. Earlier regional studies show future changes in reliability of reservoirs due to the changes in climate, projected by climate models (Brekke *et al.*, 2004; Raje and Mujumdar, 2010; Vicuna *et al.*, 2007), with some studies indicating disagreement between models on the direction of change (Brekke *et al.*, 2004). Climate models are known to disagree on the magnitude and direction of

changes in precipitation pattern among themselves (Schewe *et al.*, 2013) and compared to observations (Jones and Reid, 2001; Mcguffie *et al.*, 1999). This disagreement leads to uncertainty in the impacts of climate change on water resources (Asadieh *et al.*, 2016; Brekke *et al.*, 2004; Schewe *et al.*, 2013). However, few studies have systematically examined, at a global scale, the impact of recent and projected changes in precipitation amount and distribution on the reliability of model water supply systems designed based on past precipitation distribution.

Rainwater harvesting (RWH) has long been used as a sustainable water resource and is recognized as one of the tools of Sustainable Urban Drainage Systems (SUDS) (Mbilinyi *et al.*, 2005; Palla *et al.*, 2011). It limits the demand for potable water from other sources in urban areas as well as controlling excessive surface run-off (Helmreich and Horn, 2009; Jones and Hunt, 2010; Liaw and Tsai, 2004; Palla *et al.*, 2011; Villarreal and Dixon, 2005). Water harvesting and storage is also important in agricultural areas for increasing yields through allowing small-scale sustainable irrigation (Wisser *et al.*, 2010). Harvested precipitation is already used as a water resource, particularly in areas with arid climate, limited water resources and undeveloped water supply systems. Increasing demand for water in recent decades as well as recent interests in green infrastructure has resulted in practice of RWH in humid and/or urbanized areas as well (Jones and Hunt, 2010). The capacity to store rainwater improves the reliability of water supply as it limits the impact of temporal variability of precipitation events (Mwenge Kahinda *et al.*, 2008). However, its performance is dependent on precipitation amount and distribution (Basinger *et al.*, 2010; Fewkes, 2000).

In this paper, we analyze historical (1951-2010) changes in annual-mean and annual-maximum daily precipitation in globally distributed weather station observations (GHCN-Daily) and bias-corrected simulated precipitation from global climate models prepared under the Inter-Sectoral Impact Model Intercomparison Project (ISI-MIP), which include both the 'historical' time period 1951-2010 and the 'future' time period of 2011-2099. The high radiative forcing scenario (representative concentration pathway, RCP) RCP8.5 (Moss *et al.*, 2010) is selected for future precipitation projections, as this scenario projects the highest increase in temperature, and consequently the most distinct implication of climate change for precipitation distribution, compared to the lower radiative forcing scenarios. For sake of a fair comparison, historical climate model simulations are temporally and spatially subsampled to match the availability of

observations. A different rate of change in annual-mean and annual-maximum daily precipitation would be one indication of a change in precipitation distribution.

To quantify the possible impacts of changes in the daily precipitation distribution on water supply reliability, we consider a simple model rainwater harvesting system (RWHS). We formulate indices of RWHS specific storage capacity and specific catchment area, allowing consideration of system performance changes over time, independent of system size. This model RWHS is driven by the observational and modeled daily precipitation series to assess changes in reliability of water supply across land areas under recent and projected climate changes and relation of those to changes both in precipitation amount and in precipitation distribution. In a supplementary analysis, the precipitation times series are scaled to the amount of the first decade, before being used as inputs to the model RWHS. Through this scaled precipitation analysis, difference in system volumetric reliability in later decades for each station/grid-cell can be attributed specifically to change in precipitation distribution, controlling for change in precipitation amount.

Overall, changes in annual-mean and annual-maximum precipitation are studied along with changes in reliability of the model RWHS to investigate the impacts of changes in precipitation amount and precipitation distribution on reliability of renewable water resources. We note that the model RHWS is not intended to replicate any particular existing or proposed water supply system. This study uses the hypothetical model RWHS to investigate possible changes in water reliability across land regions due to changes in climate and consequently, precipitation distribution, and does not investigate or propose the suitability of the studied stations and regions for development of actual RWHS facilities.

Data and Methodology

The Global Historical Climatology Network (GHCN) is a database managed by the National Climatic Data Center, Arizona State University and the Carbon Dioxide Information Analysis Center. GHCN contains records from over 75000 stations in 180 countries and territories. Numerous daily variables are provided, including maximum and minimum temperature, total daily precipitation, snowfall, and snow depth; however, about two thirds of the stations report precipitation only. Both the record length and period of record vary by station and

cover intervals ranging from less than 1 year to more than 175 years (Durre *et al.*, 2010; Menne *et al.*, 2012). For analyses performed in this study, we used the GHCN-daily stations with at least 30 years of available precipitation data over the time period of 1951-2010, which includes nearly 15200 stations globally. The years with available precipitation data were defined as the ones with daily precipitation data available for at least 80 percent of the days.

The Inter-Sectoral Impact Model Intercomparison Project (ISI-MIP) (Warszawski *et al.*, 2013) provides bias-corrected daily meteorological fields, at a uniform 0.5 degree spatial resolution, from 5 selected GCMs from the fifth phase of the Coupled Model Intercomparison Project (CMIP5), which can provide the opportunity to investigate the hydrological impact of precipitation change projections from a range of GCMs after bias correction (Dankers *et al.*, 2013). The first fast-track phase of the ISI-MIP project presents outputs from the following 5 GCMs: GFDL-ESM2M, HadGEM2-ES, IPSL-CM5A-LR, MIROC-ESM-CHEM and NorESM1-M (Warszawski *et al.*, 2013), the precipitation simulations of which have been used in this study.

The GHCN observational data are station observations. However, the climate model simulations are grid-based. Climate models can simulate precipitation for all years of a specified time interval, covering all coordinates of the globe thoroughly, which is different from the spatial and temporal coverage of station observation datasets that usually cover only a certain part of the continents with missing data for a considerable number of years. This results in some difficulties in comparing climate model outputs with observations. To provide a better basis for comparison, a subsampled dataset is created for each of the 5 ISI-MIP climate models, in which each of the GHCN stations takes the modeled precipitation data of the grid-cell in which its coordinates fit. The new dataset is created with the same number of stations and same data availability pattern as GHCN. In this way of sampling model output, if GHCN dataset does not have recorded precipitation data for a specified day, the newly created dataset will not have data for that day either. The newly created dataset is called the sub-sampled ISI-MIP dataset. The subsampling is performed for each of the 5 GCMs from ISI-MIP. Hence, in total, 5 subsampled datasets are created, one for each of the GCMs, each of which has GCM-obtained daily precipitation data for the same 15200 stations as the GHCN.

Changes in Mean and Maximum precipitation

Two precipitation indices considered in this study are mean and maximum precipitation. Mean precipitation is defined as the annual-mean daily precipitation, which is the annual average of daily precipitation values. Maximum precipitation is defined as the annual-maximum daily precipitation, in which the maximum daily precipitation is selected for each year (Rx1day) (Donat *et al.*, 2013).

Precipitation time series of station observations (GHCN-daily) as well as simulations of the 5 GCMs provided by ISI-MIP are statistically analyzed to detect the trends in mean and maximum precipitation over the historical time period of 1951-2010 on global and continental scale. The relative magnitude of identified trends in mean and maximum precipitation provides some indication of changes in precipitation distribution, as well as the changes in precipitation amount. The calculations are extended for future projections of ISI-MIP climate models, under the high radiative forcing scenario RCP8.5 (Moss *et al.*, 2010), for the time period of 2011-2099 in order to investigate modeled changes in precipitation amount and distribution.

The trend slope (b) obtained from linear regression is used to quantify the strength of trends in mean and maximum precipitation time series. The relative change in precipitation is defined as the trend slope divided by the average precipitation value of the station and/or grid-cell ($b/\bar{P}$). The relative change in precipitation per K of warming is also calculated via linear regression of the natural logarithm of annual-mean or maximum precipitation against global mean near-surface temperature, which indicates the percentage change in precipitation per K global warming. To calculate this parameter for each ISI-MIP model, modeled global annual mean near-surface temperature, obtained from the corresponding CMIP5 climate model, is selected as the predictor. The global mean temperatures are from the original CMIP5 dataset and are not bias-corrected, because ISI-MIP bias-corrected fields are available only over land areas.

The trends are calculated for each station and/or model grid-cell precipitation time series. The obtained values are averaged globally as well as by continent in order to present the general trend of precipitation in different regions. For all the results obtained from the climate models, the averaging is weighted by grid cell area, meaning that the larger cells in tropics have higher impact on the average than the smaller cells in high latitudes. Continents studied comprise

Africa, Asia, Europe, North America, South America and Oceania. The subcontinent of India has results shown separately and is also included in Asia.

Model RWHS

The basic components of a simple rain water harvesting system (RWHS) are a catchment area (such as building roof), delivery system (guttering), and storage (Liaw and Tsai, 2004). Earlier studies on design of RWHS include multiple approaches such as continuous mass balance (Fewkes, 2000), non-parametric rainfall simulation (Basinger *et al.*, 2010) and statistical methods (Guo and Baetz, 2007). Behavioral analysis is considered as the most common methodology. This method simulates the inflow, outflow and change in storage volume of the rainwater harvesting system based on mass balance and simple assumptions about water demand (Fewkes and Butler, 2000; Liaw and Tsai, 2004; Palla *et al.*, 2011). In this study, a behavioral model is implemented to perform continuous simulation of a RWHS. The simulation is derived at a daily temporal resolution with precipitation observations or bias-corrected GCM simulations as input. Results of the continuous simulation are summarized in terms of volumetric system reliability in delivering the water demand.

The water release rule considered here is yield after spillage (YAS), which can be understood by considering that the demand is withdrawn at each time step, after the rainfall has been added to the storage and any spillage has taken place. The behavioral model (Figure 1) is based on daily mass balance equations:

$$Y_t = Min(D_t, S_{t-1}) \tag{1}$$

$$S_t = Min(S_{t-1} + Q_t, Ca) - Y_t \tag{2}$$

where D_t [L^3] is water demand at time t; S_t [L^3] is storage at the beginning of the tth time period; Q_t [L^3] is inflow during the tth time period; Y_t [L^3] is release during the tth time period; and Ca [L^3] is storage capacity. Assuming that the tank is covered, evaporation losses from the system as well as the incident precipitation over the tank are neglected in the mass balance equation. The inflow Q_t is evaluated as follows:

$$Q_t = Ar.P.f \tag{3}$$

where Ar [L^2] is the collection surface area, P [L] is the daily precipitation amount and f [–] is the runoff coefficient. The runoff coefficient needs field measurements to be obtained for a particular collection device, but for simplicity, the number is assumed to be constant and equal to 0.85 (Liaw and Tsai, 2004; Sturm *et al.*, 2009). We do not specifically consider quality aspects of the collected water and therefore the first flush phenomenon is disregarded (Palla *et al.*, 2011). We do not distinguish between snow and rain precipitation inputs. We assume that daily system demand is constant, which may be a reasonable approximation for domestic or industrial use; for irrigation use, a more complex formulation where demand scales with potential evaporation and depends on antecedent precipitation, as well as on cropping schedules, would be more realistic (Girvetz and Zganjar, 2014).

The performance of RWHS is generally evaluated in terms of reliability. This can be expressed as the total actual water supply divided by demand (volumetric reliability, R_v) (McMahon *et al.*, 2006). This is considered an informative index for RWHS performance (Fewkes, 2000; Liaw and Tsai, 2004; Zhang *et al.*, 2009), for which a value approaching 1 is generally desirable. R_v can be expressed mathematically as:

$$R_v = \frac{\sum_{t=1}^{N} Y_t}{\sum_{t=1}^{N} D_t} \tag{4}$$

With this model RWHS, multiplying the daily demand amount by any arbitrary factor of β and multiplying the catchment area and storage capacity by the same β factor as well will accommodate the same volumetric reliability for the system, which means the daily demand value can be excluded from the formulation (Appendix 1). Accordingly, normalizing by the demand variable, we develop a formulation for the model RWHS in terms of scaled quantities, Specific Catchment Area (A_s) and Specific Storage Capacity (C_s), defined as follows:

$$A_s = \frac{Ar \times \bar{P}}{D_t} \tag{5}$$

$$C_s = \frac{Ca}{D_t} \tag{6}$$

where A_s [-] is Specific Catchment Area; C_s [T] is Specific Storage Capacity and $\bar{P}$ is average daily precipitation over the study area [L]. The value of $\bar{P}$ is included in the definition of A_s to make it dimensionless.

The specific storage capacity (C_s) can be described as: the number of days that the water demand of the system can be supplied using the water stored in the storage. The specific catchment area (A_s) can be described as the fraction of the total demand that can be supplied using the total precipitation falling on the specified catchment area over the considered time period. $A_s=1$ corresponds to the minimum collection area necessary for the system to be able to supply the accumulated demand over the considered time period, using the accumulated precipitation, if the storage capacity is great enough that there is no spillages. Where storage is more limited, the system is not able to store and use all the precipitation collected, because of uneven distribution of the precipitation over time, and has to spill some of the precipitation, particularly if heavy rain is concentrated in a short period. Hence, an A_s value of larger than 1 is usually required to satisfy the system's demand. The exact value can be calculated based on the given precipitation time series (Appendix 1).

Changes in model RWHS volumetric reliability

Change in precipitation amount as well as precipitation distribution can result in changes in fresh water resource supply reliability, as the designed storages may not be able to hold excessive amounts of water from intense precipitation events. Study of possible changes in available sustainable water resources, induced by changes in precipitation, is accomplished here through the application of the simple model RWHS described above. The volumetric reliability (R_v) of a RWHS is representative of the capability of the system to supply the water demand from precipitation events. The expectation is that with an evenly distributed precipitation pattern, an adequately designed RWHS can capture the optimum amount or rainwater for a specified demand pattern and storage capacity. If the precipitation shifts to a more uneven distribution, for instance more intense precipitation over fewer rainy days, then even with the same total annual precipitation amount, the system will fail to capture the same amount of rainwater and would be less reliable. With constant system characteristics over time, changes in either precipitation amount or precipitation distribution can result in changes in the volumetric reliability of the RWHS.

The historical time period of 1951 to 2010 is divided into 6 decades as 1951-1960, 1961-1970… and 2001-2010, change in reliability throughout these 6 decades is studied for each station and/or grid cell. For each studied station, an individual model RWHS is designed based on the precipitation time series of that station for the 1951-1960 decade. The design parameters are the specific catchment area (A_s) and specific storage capacity (C_s). The model RHWS is sized such that the system would have R_v of 80% for that decade. The designed RWHS of the station is then kept constant and the time series of the following 5 decades are input into model and R_v of the system for each decade is calculated. Consequently, each station will have a 6-point time series of R_v. Trend in R_v at each station and/or grid-cell is calculated using linear regression, which can show any increase or decrease in R_v of the system depending on the change in amount and distribution of the precipitation.

The objective of the design procedure is to size the values of A_s and C_s such that the RWHS would have a R_v of 80% for the given precipitation time series (the first decade time series, in this case). Given A_s, C_s and precipitation time series, the value of R_v can be calculated using the behavioral model. For a decadal time frame, the values of A_s, C_s and 3652 daily precipitation values should be input into the behavioral model to calculate the corresponding value of R_v. It is not practical to analytically calculate the value of C_s for given values of R_v, A_s and precipitation. With value of R_v being defined, defining the value of A_s as well will leave the problem with only one unknown variable. As stated earlier, an A_s value of larger than 1 is usually required to completely satisfy the system's demand. Here, the value of A_s is set to be equal to 2 for all the stations. With given A_s value and precipitation time series, changing the C_s value will result in different R_v values, defining the storage-reliability curve (Appendix 1). A search process can be utilized in order to tune C_s such that the R_v value become 80%, or in other words: optimize the C_s value such that the difference between the corresponding R_v value and the target R_v value (which is 80%) be close to zero. Hence, the problem can be defined as either a nonlinear equation-solving problem or an optimization problem with one decision variable (C_s) and can be solved utilizing any optimization method. For each station, having the precipitation time series of the 1951-1960, as well as the defined values of A_s =2 and R_v =80%, the storage capacity is chosen using a metaheuristic optimization algorithm to complete the design of the model RWHS.

The target value of R_v =80% for the design procedure is selected through a sensitivity analysis. Different target values of R_v, ranging from 60% to 95% (with increments of 5%) are selected, and the design and trend analysis process are repeated for all the GHCN stations for 1951-2010. The global average of the trend in the R_v through the studied 6 decades among all the stations is then calculated. Analysis show that selection of R_v values lower than or equal to 80% (for example 70 or 75%) result in similar global trend in R_v, while selection of larger R_v target values result in sharp change in the global average value. This can be explained with the storage-capacity curve (Figure A1.b, Appendix 1), as for the high values of R_v, the required storage capacities raises drastically. Hence, selection of a high target value for R_v would result in significantly larger designed storage capacities that are more sensitive to inter-decadal precipitation fluctuations.

An increase/decrease in precipitation amount is known to respectively increase/decrease the reliability, while an impact of change in precipitation distribution associated with climate changes may also exist. Running the model RWHS with historic or scenario precipitation time series would include the impact of both changes in precipitation amount and distribution on the system reliability. We isolate the impacts of changing precipitation distribution from those of changing precipitation amount by also conducting a 'scaled' analysis in which the precipitation time series are scaled to the first decade (1951-1960), which means the precipitation time series of later decades are multiplied by a factor such that the mean precipitation of the later decades are equal to the initial decade. This results in equal total decadal precipitation input for all decades from 1951-2010, and hence the obtained difference in volumetric reliability of the system in later decades for each station/grid-cell can be attributed to the change in precipitation distribution of the area as it affects water supply reliability represented by the volumetric reliability of the model RWHS. The analysis of trend in volumetric reliability of the RWHS is performed on the GHCN stations and subsampled ISI-MIP models for 1951-2010. The design of the RWHS is separate for observation stations and each of the climate model datasets. The design of the sub-sampled ISI-MIP data is also different from the full land area ISI-MIP data, since the sub-sampled data is station-based and full data is grid-based. The analysis is further developed to the 2011-2099 time period using the ISI-MIP climate models' precipitation projections under high radiative forcing scenario (RCP8.5), using the same RHWS models designed for the 1951-2010 full ISI-MIP.

Results

Trends in Mean and Maximum precipitation for 1951-2010 and 2011-2099 (GHCN and ISI-MIP)

Table 1 presents the changes in historical mean and maximum precipitation for 1951-2010 for GHCN observational data as well as the subsampled ISI-MIP models. Table 1 presents global averages over all stations and/or grid-cells. Observation is only one dataset; hence it has one global average for each parameter. The 5 climate models give 5 global averages, of which we present the minimum, maximum, median, mean, and standard deviation in Table 1. Figure 2 illustrates the maps of average precipitation and trend for mean and maximum precipitation in GHCN stations for 1951-2010. Figure 3 illustrates the results as boxplots of trend parameters for all 5 models of ISI-MIP (full and subsampled) on global as well as continental scales for 1951-2010 and 2011-2099 (under RCP8.5 scenario) time periods, showing observations (GHCN) as colored (green and purple) markers. The boxplots show the minimum, 25th percentile, median, 75th percentile and maximum value obtained from the climate models.

On average, both observations and climate models indicate that mean and maximum precipitation have increased over 1951-2010. Table 1 shows that on global average, the subsampled ISI-MIP models show very similar mean precipitation compared to the observations. This agreement can be expected given the bias-correction procedure applied in ISI-MIP. The small value of standard deviation also indicates very good agreement among the models. In case of maximum precipitation, the observational average value of 60.83 mm day^{-1} is significantly larger than all the models. This is expected because of the spatial scale mismatch between models (0.5 degree grid cells) and observations (rain gauges representing very small areas) (Asadieh and Krakauer, 2015). As seen in the 5th and 6th columns of Table 1 and Figure 3a, both observations and models show increasing trend for mean and maximum precipitation in relative terms (% yr^{-1}), although the average increases obtained from the models are smaller than those identified in observations. Looking at the change per degree global warming, as seen in the 7th and 8th columns of Table 1 and in Figure 3d, maximum precipitation shows higher average relative change per degree warming (% K^{-1}) than mean precipitation in both observations and models. North America, Oceania, Europe, Asia, South America and Africa respectively contain about 41, 27, 13, 7, 7 and 5 % of the stations of GHCN dataset, which shows the significant

impact of the results of North America and Oceania on the global average. Figures 3a and 3d show that North America and Europe show more similar results to the global average compared to the other continents, while stations in Oceania show a wider range of trend results. The large range of trend results in continents of South America and Africa may possibly be attributed to lower density of stations in those areas compared to the other continents (Figure 2). Because of the low number of stations, these numbers may not be representative of general changes over these continents.

The global average of 10.14% increase in maximum precipitation per K global warming for the GHCN observational data is very close to the 10% per K value obtained from the HadEX2 gridded observation-based product by an earlier study (Asadieh and Krakauer, 2015), although the average value of 7.34 % K^{-1} for the subsampled bias-corrected ISI-MIP models is lower than the average value of 8.43 % K^{-1} for CMIP5 models, obtained in the aforementioned study.

Land areas with very low precipitation rates are sensitive to changes in precipitation, especially in case of climate model simulations, since very small change in the precipitation will translate in high relative change values, which may not be realistic or highly uncertain among the models. The 9th and 10th columns show the precipitation-weighted global averages of relative change per degree warming (% K^{-1}) for mean and maximum precipitation, respectively. This weighting is more sensitive to large absolute changes in precipitation amount over wet areas, rather than large relative changes over dry areas. This weighted averaging has been done using the following formula:

$$\bar{x} = \frac{\sum(x_i * GridCellArea_i * Precipitation_i)}{\sum(GridCellArea_i * Precipitation_i)}$$

where *x* represents the target parameter to be averaged for each grid cell, *GridCellArea_i* is the corresponding grid cell's area and *Precipitation_i* is the corresponding grid cell's average precipitation (mean or maximum) value for that study period. For averaging the observations and subsampled model outputs, the *GridCellArea* is eliminated from the formula since the stations do not come with defined grid cell areas. Note that regardless of the averaging procedure, the GHCN observations show a greater increase in mean precipitation over recent decades at station

locations than any of the 5 bias-corrected GCMs in ISI-MIP, while the fractional increase in maximum precipitation seen in observations is within the wide range of inter-GCM variability.

Table 2 presents average changes in historical mean and maximum precipitation for 1951-2010 for the 5 ISI-MIP climate models over the full land area (not subsampled to match with GHCN observations as in Table 1). The ISI-MIP models' global land means show lower values of average precipitation, but higher average rate of increase in precipitation (sensitive to the averaging procedure), compared to the subsampled dataset. The faster increase in maximum precipitation than mean precipitation is more distinct in full ISI-MIP model simulations. On global average, the models simulate an increase rate of 0.039% per year for mean precipitation and 0.074% per year for maximum precipitation. This is comparable with the average increase rat of 0.0775% per year in maximum precipitation for 1901-2010, obtained from 15 climate models from CMIP5 in an earlier study (Asadieh and Krakauer, 2015).

Table 3 presents the changes in future mean and maximum precipitation projected over 2011-2099 projected by the 5 ISI-MIP climate models, under the high radiative forcing scenario (RCP8.5). According to Table 3, the ISI-MIP climate models on average predict that mean precipitation would increase by 0.052 % per year. They also on average predict that maximum precipitation over land will increase faster than mean precipitation, with a rate of approximately 0.165 % per year. The first and second column of the Table 3 also indicate that climate models show better agreement on the average mean precipitation that on the average maximum precipitation, for future projections, considering the low value of standard deviation for mean precipitation. Tables 2 and 3 show that mean precipitation from the climate models increases from 2.37 mm day^{-1} for the latter half of 20th century to 2.47 mm day^{-1} for the 21st century and average maximum precipitation increases from 33.43 mm day^{-1} to 37.77 mm day^{-1}. This also indicates that in relative terms, maximum precipitation shows a faster increase than mean precipitation.

Table 1 to 3 as well as Figs 3-e and f shows that according to climate models, mean and maximum precipitation will increase at a greater rate (% per year) in future compared to the historical time period. However, maximum and mean precipitation are projected to have lower rates of increase per K warming in the future compared to the historical time period. On the other hand, considering the underestimation of observed increases seen in the historical results of the

models, it seems possible that these future changes in mean and maximum precipitation might also be underestimated (Asadieh and Krakauer, 2015).

Trends in reliability of the model RWHS driven by 1951-2010 and 2011-2099 precipitation time series (GHCN and ISI-MIP)

Table 4 presents the global average of results of the absolute change in decadal volumetric reliability (R_v) of the model RWHS applied on the GHCN observation stations as well as the 5 climate models' bias-corrected data from ISI-MIP (full and subsampled). Columns 1 to 6 show the change in volumetric reliability of the RWHS per decade (%/decade) from the initial 80% value. The percentages shown in the RWHS results represent the absolute percent change in decadal volumetric reliability (change from the initial 80%). Columns 7 to 12 show change in decadal volumetric reliability of the model RWHS per K of global warming (% K^{-1}). Results are shown for real (observed or model) precipitation as well as for scaled precipitation. Figure 4 illustrates the results shown in Table 4 as boxplots for all 5 models of ISI-MIP (full and subsampled) on global as well as continental scales for 1951-2010 and 2011-2099 (under RCP8.5 scenario) time periods, showing observations (GHCN) as colored (green and pink) markers. As seen in Figure 4, the scaled precipitation shows a smaller range of trend magnitude compare to the actual precipitation. As shown previously, mean and maximum precipitation are both increasing since 1951. Figure 3a shows that for the continents of North America, South America, Europe, Africa and Asia as well as the global average, both mean and maximum precipitation had increasing trends over 1951-2010. Figure 4a shows that for those regions, increases in the reliability of the model RWHS for the scaled precipitation are smaller than with the real precipitation. On the other hand, Figure 3a shows that Oceania had a decreasing trend in mean and maximum precipitation in GHCN observations over the last 60 years and, correspondingly, Figure 4a shows that unlike the other continents, the RWHS reliability for scaled precipitation is higher than for real precipitation for the Oceania. This illustrates that the positive/negative impact of increase/decrease in precipitation amount on model RWHS reliability is factored out by scaling the precipitation.

As seen in column 1, precipitation time series based on observations show that on global average over station locations, reliability of the hypothetical model water supply system has been increasing at a rate of 0.20% per decade for the 1951-2010 time period. However, the

subsampled climate model simulations show an average 0.15% decade^{-1} decrease in reliability, with all 5 ISI-MIP models showing decreasing reliability. Table 4 also shows that in observations, the reliability increases at a rate of 2.34% per K of global warming. This is however quite different than the results of the subsampled ISI-MIP, which shows an average 0.60% decrease in the reliability per K warming.

Driving the model RWHS with scaled precipitation based on observations yields on global average, that reliability has been increasing at a rate of 0.11% per decade for the 1951-2010 time period while the subsampled ISI-MIP simulations show an average 0.13% decade^{-1} decrease in the reliability. Table 4 also shows that in observations, the reliability of the model RWHS driven by scaled precipitation increases at a rate of 1.44% per K of global warming, which is different than the results of the subsampled ISI-MIP with an average 0.68% decrease in the reliability per K warming. Thus, the model RWHS driven by real and scaled precipitation show that ISI-MIP climate models shows an opposite (decreasing) average reliability trend from that calculated using GHCN precipitation observations.

The RWHS model driven by full land area ISI-MIP data also yields decreasing trend in reliability for both real and scaled precipitation, with lower rate that the subsampled ISI-MIP (Table 4, columns 3-4), even though the mean and maximum precipitation shows increasing trend in that time period (Table 2). However, as stated earlier, the rate of increase in maximum precipitation is almost double the rate of mean precipitation (Table 2). The ISI-MIP models project that for the future time period of 2011-2099 under high radiative forcing scenario (RCP8.5), the volumetric reliability of the model RWHS when driven by real as well as scaled precipitation will decrease (Table 4, columns 5-6), even though the models project increasing trends for mean and maximum precipitation for that time period (Table 2). However, similar to the historical period, the rate of increase in maximum precipitation is significantly greater than the rate of increase in mean precipitation for future precipitation projections (Table 2). Figure 5 shows global maps of changes in decadal volumetric reliability (R_v) of the RWHS system in absolute terms (% decade^{-1}) as well as per K of global warming (% K^{-1}), for real and scaled precipitation, for GHCN observation stations over 1951-2010.

As another way of disaggregating the changes in precipitation and model RWHS reliability seen around the world, Figures 6 and 7 depict the average relative change in mean and maximum

precipitation (% decade^{-1}) for different precipitation deciles, as well as the absolute change in decadal volumetric reliability (% decade^{-1}) for real and scaled precipitation, for the same precipitation deciles. The lowest deciles represent the driest areas and the highest deciles represent the wettest areas. Deciles are calculated based on the average precipitation during each study period. Figure 7 shows the average results of the 5 climate models for full land area ISI-MIP data for 1951-2010 and 2011-2011 time periods. Figure 6a shows that for historical climate model simulations, the precipitation increase rates for dry precipitation deciles are higher than the higher ones. However, the rate of increase in maximum precipitation is lower than mean precipitation for the initial deciles and becomes greater than the mean precipitation, as the deciles go higher. Correspondingly, Figure 6b shows that the RWHS reliability has increased for the driest deciles and the trend decreases as areas become wetter. As seen in the figure, the wettest precipitation deciles have the largest difference between mean and maximum precipitation change rate and the reliability changes of the model RWHS there are negative. Climate models simulations show that for the dry precipitation deciles where the difference between maximum and mean precipitation change rate is not as high as the wet deciles, the significant increase in precipitation amount overpowers the smaller change in the precipitation distribution and results in increased reliability. Similar pattern is seen for the future 2011-2099 precipitation projections (Figs. 6c and d). This further indicates the impact of change in precipitation distribution on the reliability of water supplies.

Figure 7 presents change in mean and maximum precipitation as well as model RWHS reliability by precipitation deciles, for GHCN station observations and average of the 5 subsampled ISI-MIP climate models, for 1951-2010. Figure 7a shows the relative change in mean and maximum precipitation for GHCN stations (% decade^{-1}). The GHCN shows increasing trend for both mean and maximum precipitation, with the rate of change being higher for the wetter deciles. Lower (drier) deciles show greater increase in mean than maximum precipitation. However, the higher deciles generally show greater increase for maximum than mean precipitation. Despite the full ISI-MIP models, the model RHWS driven by GHCN observations show increase in reliability for low and high deciles, and decrease for some middle deciles. However, the difference between rate of change in mean and maximum precipitation is more significant in ISI-MIP models than the GHCN observations. Figure 7c shows that for all precipitation deciles, the subsampled ISI-MIP models simulate significantly faster increase in

maximum precipitation than mean precipitation. Correspondingly, Figure 7d shows that a decreasing trend in modeled volumetric reliability for all those deciles. Figures 6 and 7 illustrate that for climate model precipitation simulations, for the precipitation deciles which the maximum precipitation is increasing faster than the mean precipitation, the reliability of the model RWHS driven by those precipitation time series decreases, or at least increases less rapidly than the other deciles. However, the observational precipitation records of the GHCN do not show that behavior, as the reliability increases for most deciles. Figs. 6b and 7d show that for the full and subsampled ISI-MIP, the volumetric reliability decreases more in wet areas (the higher deciles), so that driving the model RWHS with ISI-MIP models misses the increasing reliability trend implied by observations over wetter parts of the land surface. Average of relative change in decadal volumetric reliability of the RWHS system per K of global warming (% K^{-1}) for different precipitation deciles also shows similar patterns as the trend in absolute reliability.

Discussion

Both observations and climate models indicate that mean and maximum precipitation averaged over land areas increased since 1951, although the average trend magnitudes obtained from the models are smaller than those identified in observations. Maximum precipitation shows higher rate of relative change per degree warming (% K^{-1}) than mean precipitation in both observations and models. The difference between change in mean and maximum precipitation is larger in models, compared to the observations: The modeled subsampled global average of relative change per degree warming for mean precipitation is 1.36% K^{-1} which is considerably smaller than the 7.34% K^{-1} for maximum precipitation, while observations show 7.64 and 10.14% K^{-1} increase for mean and maximum precipitation, respectively. Earlier studies have used energy balance considerations to explain this pattern seen in GCMs, that unlike the impact of global warming on rate of increase in maximum precipitation, which is expected to be close to the Clausius-Clapeyron equation slope of approximately 7% per K warming (Asadieh and Krakauer, 2015; Pall *et al.*, 2006), the mean precipitation increases at a slower rate around 2% K^{-1} (Held and Soden, 2006). However, the GHCN observations show a higher rate of increase in precipitation per K global warming compared to GCM simulations of the same time period, especially for mean precipitation. One possible reason for this discrepancy may be that considerations of thermodynamics and large-scale circulation are valid in the global average,

while the GHCN data covers only parts of the land surface, primarily North America, Europe, North and East Asia and Oceania. However, subsampling the GCM output shows that, at least where there are station observations, observed trends are not well captured.

Precipitation observations imply that on global average, reliability of the model precipitation-driven water supply system under assumed temporally constant demand has been increasing at a rate of 0.2% each decade for the 1951-2010 time period, a 2.34% increase per K of global warming. However, the subsampled climate models simulations show an average 0.15% per decade (0.60% per K) decrease in reliability. Scaling the later decades as the initial 1951-1960 decade would result in equal total annual precipitation for all decades from 1951-2010 and hence the difference in volumetric reliability of the system in different decades for each station/grid-cells can be attributed to the change in precipitation distribution (as opposed to mean amount) and its effect on water supply reliability. Our results show that for continents with increasing/decreasing trend in precipitation, the reliability of the model RWHS with scaled precipitation is respectively smaller/larger than with actual precipitation. This confirms that the respective positive/negative impact of increase/decrease in precipitation amount on RWHS reliability is factored out by scaling the precipitation. Observations show that for scaled observed precipitation, on global average, reliability of the model RWHS has been increasing more slowly, compared to the observed-precipitation driven RWHS, at a rate of 0.11% per decade for the 1951-2010 time period. Subsampled climate models show a decrease in the reliability of RWHS driven by scaled precipitation, with an average 0.13% per decade decrease in reliability. Thus, the model RWHS driven by real and scaled precipitation show that ISI-MIP climate models shows an opposite (decreasing) average reliability trend from that calculated using GHCN precipitation observations.

Analyses of the full land area GCM simulations show even faster increase in maximum precipitation than mean precipitation, for the historical period. The RWHS model driven by full land area ISI-MIP data also yields decreasing trend in reliability for both real and scaled precipitation, with lower rate that the subsampled ISI-MIP, even though the mean and maximum precipitation shows increasing trend in that time period. The considered GCMs project for the RCP8.5 forcing scenario that in the 21st century, mean precipitation will have an increasing trend of approximately 0.052 % per year on average. Also, the GCMs project that maximum precipitation would increase significantly faster than mean precipitation in the future, with a rate

of approximately 0.165 % per year. This is greater than the rate of change in both subsampled and full land area simulations in the historical time period. The ISI-MIP models project that for the future time period of 2011-2099, the volumetric reliability of the model RWHS when driven by real as well as scaled precipitation will decrease, at a greater rate than for the historical time period and with wider disagreement between models.

Analysis of historical and future full land area ISI-MIP climate model simulations in different precipitation percentiles indicates that for the precipitation deciles where maximum precipitation has not increased much faster than mean precipitation (usually the driest areas), the model RWHS reliability has increased. This may be attributed to the increase in precipitation amount and little change in precipitation distribution. However, for the precipitation deciles where maximum precipitation is increasing faster than mean precipitation (usually the wettest areas), the model RWHS reliability has decreased. This implies that the climate models suggest that for the areas with large increases in the ratio of maximum to mean precipitation, the reliability of the precipitation-fed water supplies decreases, even though the precipitation amount has increased.

Our RWHS driven by observational precipitation shows increased mean reliability. Observational precipitation shows faster increase in maximum than mean precipitation, but the difference between rate of change in mean and maximum precipitation is less significant than in the climate models. However, results show that on global average, the reliability of the model RWHS is improving even when the precipitation time series are scaled to remove the impact of increasing mean precipitation. The increasing reliability of RWHS at station locations that is implied by observations may be explained by a more even distribution of precipitation either between seasons or within seasons, despite the observed disproportionate increase in the intensity of the heaviest daily precipitation. However, subsampled ISI-MIP climate models show a decreasing trend in the model RWHS reliability, suggesting that the current generation of GCMs is not accurately representing aspects of precipitation distribution that are important from a water resources perspective. A previous analysis suggests that observations are consistent with GCMs in showing dry seasons getting relatively dryer compared to wet seasons (Chou *et al.*, 2013). An analysis using station data over the USA, however, finds increases in precipitation frequency during both wet and dry seasons and a decrease in length of dry spells over 1930-2009 (Pal *et al.*, 2013). A recent comprehensive analysis of different observation-based data sets over

land finds that the "wet gets wetter, dry gets dryer" paradigm for the effect of global warming on aridity indices is not generally valid for land areas (Greve *et al.*, 2014). Biases in representation of precipitation seasonality, including wet season length, in current GCMs have also been studied (Pascale *et al.*, 2014). Clearly, further work is needed to better understand the disagreement found here between GCMs and observations and its relevance to the reliability of different water supplies (e.g. runoff-fed, versus directly precipitation-fed, reservoir systems (Huang *et al.*, 2014)).

Changes in precipitation distribution can result in increased intensity and frequency of flood and drought events and also can affect the availability of fresh water resources, which requires consideration of both precipitation amount and distribution changes in order to design reliable water supply systems. Climate models are known to disagree, among themselves and compared to observations, on the magnitude and direction of changes in precipitation amount and distribution. The present study shows that the ISI-MIP climate models show different direction of change in reliability of a simple water supply system than available station observations, although they capture the correct sign of change in precipitation amount.

The model RWHS used here to compare globally the consequences of observed and modeled precipitation changes for supply reliability is not intended to represent any particular actual water supply and, for local studies, could be replaced by more sophisticated models that better represent the types of water supply of interest to decision making in a particular jurisdiction. Based on the present study, we suggest that the future precipitation projections of climate models should generally be used with caution for water resources system designs, and that more effort needs to be made to understand how to accurately model the physical mechanisms for changes in precipitation distribution, as well as in mean amount, if climate model projections are to be more useful in designing water supplies to perform well under future climate change.

Conclusion

Maximum precipitation is increasing faster than mean precipitation in both observations and model simulations. This can be interpreted as one index of change in precipitation distribution in which a larger fraction of annual precipitation is falling in the heaviest events. The

expectation might be that such changes in precipitation distribution would lead to less capability of storages in capturing rainwater and hence, less reliable precipitation-fed water supply. Climate model simulated precipitation series suggest that for areas with little change in precipitation distribution, increase in precipitation leads to increasing water supply reliability, while for areas with significant change in precipitation distribution, the reliability of the precipitation-fed water supplies is tending to decrease, even where the mean precipitation amount has increased. However, our results show that on global average, the reliability of a model RWHS driven by observed daily station precipitation inputs is increasing. Climate models underestimate the increasing trends in mean and maximum precipitation and also imply the opposite direction of change in reliability of the model water supply system compared to the observations: the model RHWS driven by climate models' simulated daily precipitation show a decreasing trend in reliability of water supply. We do suggest further investigation of the impact of change in precipitation distribution on water supply reliability, using other indices of distribution change.

Climate models predict that mean and maximum precipitation would continue to increase, under a high radiative forcing scenario, with faster trend for maximum precipitation than mean precipitation and that the model RWHS driven by modeled daily precipitation would on average show a decreasing trend in water supply reliability. However, comparison of historical results between observations and models suggest that the current generation of climate models is not accurately representing aspects of precipitation distribution that are important from a water resources perspective. These systematic mismatches for the recent decades suggest the need for caution in using precipitation trend scenarios derived from climate models as a basis for designing water supply systems.

Appendix 1: Specific Catchment Area and Specific Storage

In this appendix, we use a 30-year historical precipitation time series of a sample station extracted from GHCN-daily in order to illustrate the performance of the implemented model RWHS in regard to volumetric reliability. Figure A1.a illustrates the volumetric reliability of the model RWHS for different demand values. The daily demand of the building, to be provided by the system, is assumed for the sake of illustration to be either 0.2 m^3 (200 liters) or 0.4 m^3 (400 liters) (Figure A1.a). We also simulate different values of building catchment area, ranging from

50 m^2 for a small building to 200 m^2. Figure A1.a illustrates that as the tank storage capacity increases, the performance of the system, measured by volumetric reliability, improves. It also can be seen from the Figure that larger catchment areas allow smaller tank sizes for the same system reliability.

[INSERT FIGURE A1 IN HERE, OR SOMWHERE IN THIS APPENDIX]

Table A1 presents the minimum values of tank storage capacity for a volumetric reliability (R_v) of 95%, for various combinations of daily demand and catchment area. As an example, the RWHS in a building with catchment area of 200 m^2 and tank size of 5 m^3 would be able to supply a daily water demand of 0.3 m^3 for the building with 95% reliability. As seen from the Table and also logically expected, higher water demands require larger tanks to support the demand of the system with any given (in this case 95%) reliability. Small catchment areas support high water demands only with huge tank sizes for the system, while catchment areas smaller than a threshold cannot provide a 95% reliability for the system with any tank size, as seen in the Table as well as Figure 2a, where a 50 m^2 area is not enough to gather sufficient amount of water for daily water demands of 0.3 m^3 or higher.

[INSERT TABLE A1 IN HERE, OR SOMWHERE IN THIS APPENDIX]

Figure A1.a as well as Table A1 show that for a daily demand of 0.2 m^3 and catchment area of 100 m^2, tank storage capacity of 4.5 m^3 will accommodate a volumetric reliability of 95%. On the other hand, for a daily demand of 0.4 m^3 and catchment area of 200 m^2, storage capacity of 9 m^3 will result in 95% volumetric reliability. As another instance, for a daily demand of 0.2 m^3 and catchment area of 100 m^2, tank storage capacity of 1.25 m^3 will accommodate a volumetric reliability of 70%, where for a daily demand of 0.4 m^3 and catchment area of 200 m^2, storage capacity of 2.5 m^3 will result in the same 70% volumetric reliability. This illustrates that, with doubling the daily demand amount, doubling both the catchment area and storage capacity as well will accommodate the same volumetric reliability for the system, which means the daily demand value can be eliminated from the aforementioned curves for a standardized formulation.

Accordingly, we developed a formulation for the model RWHS in terms of scaled quantities, specific catchment area (A_s) and specific storage capacity (C_s), defined as follows:

$$A_s = \frac{A_r \times \bar{P}}{D_t} \tag{A1}$$

$$C_s = \frac{C_a}{D_t} \tag{A2}$$

where A_r is the catchment area [dimensions: L^2], C_a is the storage capacity [L^3] and D_t is the water demand [$L^3\,T^{-1}$]. A_s [-] is specific catchment area; C_s [T] is specific storage capacity and $\bar{P}$ is average daily precipitation over the study area and study time period [$L\,T^{-1}$]. The value of $\bar{P}$ is included in the definition of A_s to make it dimensionless.

Reconsidering the examples described before, with average daily precipitation equal to 4 mm day^{-1} and volumetric reliability of 95%, a specific catchment area of 2 will have the corresponding specific storage value of 22.5 days under the meteorological conditions of the Puerto Rico station, regardless of daily demand value being 0.2 or 0.4 m^3 or any other amount. Likewise, for volumetric reliability of 70%, a specific catchment area of 2 will have the corresponding specific storage value of 6.25 days, for any daily demand values. Figure A1.b then depicts the curves of volumetric reliability (R_v) of the system versus specific storage capacity (day) at various specific catchment area values, obtained from the newly developed indices. Figures A1.b, or its equivalent constructed for any other desired area, could be utilized in designing the tank size of the model RWHS to meet a particular reliability target, for any assumed demand.

Acknowledgements

Literatures Cited

Allan, R.P. and B.J. Soden, 2008. Atmospheric Warming and the Amplification of Precipitation Extremes. Science 321:1481–484, DOI:10.1126/science.1160787.

Allen, M.R. and W.J. Ingram, 2002. Constraints on Future Changes in Climate and the Hydrologic Cycle. Nature 419:224–232, DOI:10.1038/nature01092.

Arnell, N.W., 2004. Climate Change and Global Water Resources: SRES Emissions and Socio-Economic Scenarios. Global Environmental Change 14:31–52, DOI:10.1016/j.gloenvcha.2003.10.006.

Asadieh, B. and N.Y. Krakauer, 2015. Global Trends in Extreme Precipitation: Climate Models versus Observations. Hydrology and Earth System Sciences 19:877–891, DOI:10.5194/hess-19-877-2015.

Asadieh, B., N.Y. Krakauer, and B.M. Fekete, 2016. Historical Trends in Mean and Extreme Runoff and Streamflow Based on Observations and Climate Models. Water 8:189, DOI:10.3390/w8050189.

Basinger, M., F. Montalto, and U. Lall, 2010. A Rainwater Harvesting System Reliability Model Based on Nonparametric Stochastic Rainfall Generator. Journal of Hydrology 392:105–118, DOI:10.1016/j.jhydrol.2010.07.039.

Brekke, L.D., E.P. Maurer, J.D. Anderson, M.D. Dettinger, E.S. Townsley, A. Harrison, and T. Pruitt, 2009. Assessing Reservoir Operations Risk under Climate Change. Water Resources Research 45:1–16, DOI:10.1029/2008WR006941.

Brekke, L.D., N.L. Miller, K.E. Bashford, N.W.T. Quinn, and J. a. Dracup, 2004. Climate Change Impacts Uncertainty for Water Resources in the San Joaquin River Basin, California. Journal of the American Water Resources Association 40:149–164, DOI:10.1111/j.1752-1688.2004.tb01016.x.

Chou, C., J.C.H. Chiang, C.-W. Lan, C.-H. Chung, Y.-C. Liao, and C.-J. Lee, 2013. Increase in the Range between Wet and Dry Season Precipitation. Nature Geoscience 6:263–267, DOI:10.1038/ngeo1744.

Dankers, R., N.W. Arnell, D.B. Clark, P.D. Falloon, B.M. Fekete, S.N. Gosling, J. Heinke, H. Kim, Y. Masaki, Y. Satoh, T. Stacke, Y. Wada, and D. Wisser, 2013. First Look at Changes in Flood Hazard in the Inter-Sectoral Impact Model Intercomparison Project Ensemble. Proceedings of the National Academy of Sciences 111:3257–3261, DOI:10.1073/pnas.1302078110.

Donat, M.G., L. V. Alexander, H. Yang, I. Durre, R. Vose, R.J.H. Dunn, K.M. Willett, E. Aguilar, M. Brunet, J. Caesar, B. Hewitson, C. Jack, a. M.G. Klein Tank, a. C. Kruger, J. Marengo, T.C. Peterson, M. Renom, C. Oria Rojas, M. Rusticucci, J. Salinger, a. S. Elrayah, S.S. Sekele, a. K. Srivastava, B. Trewin, C. Villarroel, L. a. Vincent, P. Zhai, X. Zhang, and S. Kitching, 2013. Updated Analyses of Temperature and Precipitation Extreme Indices since the Beginning of the Twentieth Century: The HadEX2 Dataset. Journal of Geophysical Research: Atmospheres 118:2098–2118, DOI:10.1002/jgrd.50150.

Durre, I., M.J. Menne, B.E. Gleason, T.G. Houston, and R.S. Vose, 2010. Comprehensive Automated Quality Assurance of Daily Surface Observations. Journal of Applied Meteorology and Climatology 49:1615–1633, DOI:10.1175/2010JAMC2375.1.

Fewkes, A., 2000. Modelling the Performance of Rainwater Collection Systems: Towards a Generalised Approach. Urban Water 1:323–333, DOI:10.1016/S1462-0758(00)00026-1.

Fewkes, A. and D. Butler, 2000. Simulating the Performance of Rainwater Collection and Reuse Systems Using Behavioural Models. Building Services Engineering Research and Technology 21:99–106, DOI:10.1177/014362440002100204.

Field, C.B., 2012. Managing the Risks of Extreme Events and Disasters to Advance Climate Change Adaptation: Special Report of the Intergovernmental Panel on Climate Change. Cambridge University Press, Cambridge, UK.

Fowler, H.J., C.G. Kilsby, and P. E. O'Connell, 2003. Modeling the Impacts of Climatic Change and Variability on the Reliability, Resilience, and Vulnerability of a Water Resource System. Water Resources Research 39. DOI:10.1029/2002WR001778.

Girvetz, E.H. and C. Zganjar, 2014. Dissecting Indices of Aridity for Assessing the Impacts of Global Climate Change. Climatic Change 126:469–483, DOI:10.1007/s10584-014-1218-9.

Greve, P., B. Orlowsky, B. Mueller, J. Sheffield, M. Reichstein, and S.I. Seneviratne, 2014. Global Assessment of Trends in Wetting and Drying over Land. Nature Geoscience 7:716–721, DOI:10.1038/ngeo2247.

Guo, Y. and B. Baetz, 2007. Sizing of Rainwater Storage Units for Green Building Applications. Journal of Hydrologic Engineering 12:197–205.

Hanson, L.S. and R.M. Vogel, 2014. Generalized Storage–reliability–yield Relationships for Rainwater Harvesting Systems. Environmental Research Letters 9:075007, DOI:10.1088/1748-9326/9/7/075007.

Held, I.M. and B.J. Soden, 2006. Robust Responses of the Hydrological Cycle to Global Warming. Journal of Climate 19:5686–5699, DOI:10.1175/JCLI3990.1.

Helmreich, B. and H. Horn, 2009. Opportunities in Rainwater Harvesting. Desalination 248:118–124, DOI:10.1016/j.desal.2008.05.046.

Huang, J.-C., T.-Y. Lee, and J.-Y. Lee, 2014. Observed Magnified Runoff Response to Rainfall Intensification under Global Warming. Environmental Research Letters 9:034008, DOI:10.1088/1748-9326/9/3/034008.

Jones, M.P. and W.F. Hunt, 2010. Performance of Rainwater Harvesting Systems in the Southeastern United States. Resources, Conservation and Recycling 54:623–629, DOI:10.1016/j.resconrec.2009.11.002.

Jones, P.D. and P. a. Reid, 2001. Assessing Future Changes in Extreme Precipitation over Britain Using Regional Climate Model Integrations. International Journal of Climatology 21:1337–1356, DOI:10.1002/joc.677.

Karl, T.R., J.M. Melillo, and T.C. Peterson, 2009. Global Climate Change Impacts in the United States. Cambridge University Press, New York, USA. http://medcontent.metapress.com/index/A65RM03P4874243N.pdf. Accessed 14 Jan 2014.

Kumar, S. and D. Lawrence, 2014. Less Reliable Water Availability in the 21st Century Climate Projections. Earth's Future 2:152–160, DOI:10.1002/2013EF000159.Abstract.

Lambert, F.H., A.R. Stine, N.Y. Krakauer, and J.C.H. Chiang, 2008. How Much Will Precipitation Increase with

Global Warming? Eos, Transactions American Geophysical Union 89:193–194, DOI:10.1029/2008EO210001.

Li, G., S.P. Harrison, P.J. Bartlein, K. Izumi, and I. Colin Prentice, 2013. Precipitation Scaling with Temperature in Warm and Cold Climates: An Analysis of CMIP5 Simulations. Geophysical Research Letters 40:4018–4024, DOI:10.1002/grl.50730.

Liaw, C. and Y.-L. Tsai, 2004. Optimum Storage Volume of Rooftop Rain Water Harvesting Systems for Domestive Use. JAWRA Journal of the American Water Resources Association 40:901–912, DOI:10.1111/j.1752-1688.2004.tb01054.x.

Liu, C. and R.P. Allan, 2013. Observed and Simulated Precipitation Responses in Wet and Dry Regions 1850–2100. Environmental Research Letters 8:034002, DOI:10.1088/1748-9326/8/3/034002.

Mbilinyi, B.P., S.D. Tumbo, H.F. Mahoo, E.M. Senkondo, and N. Hatibu, 2005. Indigenous Knowledge as Decision Support Tool in Rainwater Harvesting. Physics and Chemistry of the Earth 30:792–798, DOI:10.1016/j.pce.2005.08.022.

Mcguffie, K., N. Holbrook, Z. Kothavala, O. Balachova, and J. Hoekstra, 1999. Assessing Simulations of Daily Temperature and Precipitation Variability With Global Climate Models. International Journal of Climatology 19:1–26.

McMahon, T. a., A.J. Adeloye, and S.-L. Zhou, 2006. Understanding Performance Measures of Reservoirs. Journal of Hydrology 324:359–382, DOI:10.1016/j.jhydrol.2005.09.030.

Menne, M.J., I. Durre, R.S. Vose, B.E. Gleason, and T.G. Houston, 2012. An Overview of the Global Historical Climatology Network-Daily Database. Journal of Atmospheric and Oceanic Technology 29:897–910, DOI:10.1175/JTECH-D-11-00103.1.

Min, S.-K., X. Zhang, F.W. Zwiers, and G.C. Hegerl, 2011. Human Contribution to More-Intense Precipitation Extremes. Nature 470:378–81, DOI:10.1038/nature09763.

Moss, R.H., J. a Edmonds, K. a Hibbard, M.R. Manning, S.K. Rose, D.P. van Vuuren, T.R. Carter, S. Emori, M. Kainuma, T. Kram, G. a Meehl, J.F.B. Mitchell, N. Nakicenovic, K. Riahi, S.J. Smith, R.J. Stouffer, A.M. Thomson, J.P. Weyant, and T.J. Wilbanks, 2010. The next Generation of Scenarios for Climate Change Research and Assessment. Nature 463:747–756, DOI:10.1038/nature08823.

Mwenge Kahinda, J.M., E.S.B. Lillie, a. E. Taigbenu, M. Taute, and R.J. Boroto, 2008. Developing Suitability Maps for Rainwater Harvesting in South Africa. Physics and Chemistry of the Earth 33:788–799, DOI:10.1016/j.pce.2008.06.047.

O'Gorman, P.A. and T. Schneider, 2009. The Physical Basis for Increases in Precipitation Extremes in Simulations of 21st-Century Climate Change. Proceedings of the National Academy of Sciences 106:14773–14777, DOI:10.1073/pnas.0907610106.

Oki, T. and S. Kanae, 2006. Global Hydrological Cycles and World Water Resources. Science 313:1068–1072,

DOI:10.1126/science.1128845.

Pal, I., B.T. Anderson, G.D. Salvucci, and D.J. Gianotti, 2013. Shifting Seasonality and Increasing Frequency of Precipitation in Wet and Dry Seasons across the U.S. Geophysical Research Letters 40:4030–4035, DOI:10.1002/grl.50760.

Pall, P., M.R. Allen, and D.A. Stone, 2006. Testing the Clausius–Clapeyron Constraint on Changes in Extreme Precipitation under CO2 Warming. Climate Dynamics 28:351–363, DOI:10.1007/s00382-006-0180-2.

Palla, a., I. Gnecco, and L.G. Lanza, 2011. Non-Dimensional Design Parameters and Performance Assessment of Rainwater Harvesting Systems. Journal of Hydrology 401:65–76, DOI:10.1016/j.jhydrol.2011.02.009.

Pascale, S., V. Lucarini, X. Feng, A. Porporato, and S.U. Hasson, 2014. Analysis of Rainfall Seasonality from Observations and Climate Models. Climate Dynamics:1–21, DOI:10.1007/s00382-014-2278-2.

Payne, J., A. Wood, and A. Hamlet, 2004. Mitigating the Effects of Climate Change on the Water Resources of the Columbia River Basin. Climatic Change 62:233–256, DOI:10.1023/B:CLIM.0000013694.18154.d6.

Polson, D., G.C. Hegerl, R.P. Allan, and B.B. Sarojini, 2013. Have Greenhouse Gases Intensified the Contrast between Wet and Dry Regions? Geophysical Research Letters 40:4783–4787, DOI:10.1002/grl.50923.

Raje, D. and P.P. Mujumdar, 2010. Reservoir Performance under Uncertainty in Hydrologic Impacts of Climate Change. Advances in Water Resources 33:312–326, DOI:10.1016/j.advwatres.2009.12.008.

Ricko, M., R.F. Adler, and G.J. Huffman, 2016. Climatology and Interannual Variability of Quasi-Global Intense Precipitation Using Satellite Observations. Journal of Climate. DOI:10.1175/JCLI-D-15-0662.1, DOI:10.1175/JCLI-D-15-0662.1.

Schewe, J., J. Heinke, D. Gerten, I. Haddeland, N.W. Arnell, D.B. Clark, R. Dankers, S. Eisner, B.M. Fekete, F.J. Colón-González, S.N. Gosling, H. Kim, X. Liu, Y. Masaki, F.T. Portmann, Y. Satoh, T. Stacke, Q. Tang, Y. Wada, D. Wisser, T. Albrecht, K. Frieler, F. Piontek, L. Warszawski, and P. Kabat, 2013. Multimodel Assessment of Water Scarcity under Climate Change. Proceedings of the National Academy of Sciences. DOI:10.1073/pnas.1222460110, DOI:10.1073/pnas.1222460110.

Solomon, S., D. Qin, M. Manning, M. Marquis, K. Averyt, M.M.B. Tignor, H.L. Miller, and Z. Chen, 2007. Climate Change 2007 : The Physical Science Basis, Contribution of Working Group I to the Fourth Assessment Report of the Intergovernmental Panel on Climate Change. Cambridge University Press, Cambridge, United Kingdom and New York, NY, USA,.

Stocker, T.F., D. Qin, G.-K. Plattner, M.M.B. Tignor, S.K. Allen, J. Boschung, A. Nauels, Y. Xia, V. Bex, and P.M. Midgley, 2013. Climate Change 2013: The Physical Science Basis. Working Group I Contribution to the Fifth Assessment Report of the Intergovernmental Panel on Climate Change-Abstract for Decision-Makers. Cambridge University Press.

Sturm, M., M. Zimmermann, K. Schütz, W. Urban, and H. Hartung, 2009. Rainwater Harvesting as an Alternative Water Resource in Rural Sites in Central Northern Namibia. Physics and Chemistry of the Earth, Parts A/B/C

34:776–785, DOI:10.1016/j.pce.2009.07.004.

Su, M.-D., C.-H. Lin, L.-F. Chang, J.-L. Kang, and M.-C. Lin, 2009. A Probabilistic Approach to Rainwater Harvesting Systems Design and Evaluation. Resources, Conservation and Recycling 53:393–399, DOI:10.1016/j.resconrec.2009.03.005.

Trenberth, K.E., 2011. Changes in Precipitation with Climate Change. Climate Research 47:123–138, DOI:10.3354/cr00953.

Trenberth, K.E., A. Dai, R.M. Rasmussen, and D.B. Parsons, 2003. The Changing Character of Precipitation. Bulletin of the American Meteorological Society 84:1205–1217, DOI:10.1175/BAMS-84-9-1205.

Trenberth, K.E., J. Fasullo, and L. Smith, 2005. Trends and Variability in Column-Integrated Atmospheric Water Vapor. Climate Dynamics 24:741–758, DOI:10.1007/s00382-005-0017-4.

Vicuna, S., E.P. Maurer, B. Joyce, J. a Dracup, and D. Purkey, 2007. The Sensitivity of California Water Resources To Climate Change Scenarios. Journal of the American Water Resources Association 43:482–498, DOI:10.1111/j.1752-1688.2007.00038.x.

Villarreal, E.L. and A. Dixon, 2005. Analysis of a Rainwater Collection System for Domestic Water Supply in Ringdansen, Norrköping, Sweden. Building and Environment 40:1174–1184, DOI:10.1016/j.buildenv.2004.10.018.

Vörösmarty, C.J., P. Green, J. Salisbury, and R.B. Lammers, 2000. Global Water Resources: Vulnerability from Climate Change and Population Growth. Science 289:284–288, DOI:10.1126/science.289.5477.284.

Warszawski, L., K. Frieler, V. Huber, F. Piontek, O. Serdeczny, and J. Schewe, 2013. The Inter-Sectoral Impact Model Intercomparison Project (ISI-MIP): Project Framework. Proceedings of the National Academy of Sciences 111:1–5, DOI:10.1073/pnas.1312330110.

Wentz, F.J., L. Ricciardulli, K. Hilburn, and C. Mears, 2007. How Much More Rain Will Global Warming Bring? Science 317:233–235, DOI:10.1126/science.1140746.

Wisser, D., S.E. Frolking, E.M. Douglas, B.M. Fekete, A.H. Schumann, and C.J. Vörösmarty, 2010. The Significance of Local Water Resources Captured in Small Reservoirs for Crop Production - a Global-Scale Analysis. Journal of Hydrology 384:264–275, DOI:10.1016/j.jhydrol.2009.07.032.

Wu, P., N. Christidis, and P. Stott, 2013. Anthropogenic Impact on Earth's Hydrological Cycle. Nature Climate Change 3:807–810, DOI:10.1038/nclimate1932.

Zhang, Y., D. Chen, L. Chen, and S. Ashbolt, 2009. Potential for Rainwater Use in High-Rise Buildings in Australian Cities. Journal of Environmental Management 91:222–6, DOI:10.1016/j.jenvman.2009.08.008.

Tables

Table 1. Global-averaged results of annual-mean and annual-maximum precipitation trend analysis, for the GHCN station observation data and the 5 subsampled ISI-MIP climate models, from 1951 to 2010. The 5 ISI-MIP models give 5 global averages, of which the minimum, maximum, median, mean, and standard deviation are presented.

	Average of precipitation (P) (mm day^{-1})		Slope of Change (b) (mm day^{-1} year^{-1})		Relative change in precipitation (b/P) (% year^{-1})		Change per K global warming – Absolute value Average (% K^{-1})		Change per K global warming – Precipitation weighted Average (% K^{-1})	
	Mean precip.	Max. precip.	Mean precip.	Max. precip.	Mean precip.	Max. precip.	Mean precip.	Max. precip.	Mean precip.	Max. precip.
GHCN	2.21	60.83	0.0017	0.0371	0.075	0.070	7.64	10.14	6.52	8.71
ISI-MIP average	2.40	39.90	0.0000	0.0205	0.003	0.055	1.36	7.34	1.10	7.73
ISI-MIP min.	2.39	33.52	-0.0015	-0.0100	-0.069	-0.013	-1.98	1.65	-2.63	1.33
ISI-MIP max.	2.41	45.93	0.0013	0.0733	0.052	0.165	4.72	11.85	4.93	12.02
ISI-MIP median	2.40	40.47	-0.0003	0.0086	0.011	0.021	1.78	7.71	1.95	9.00
ISI-MIP St.Dev.	0.01	5.11	0.0011	0.0325	0.047	0.073	3.17	3.70	3.18	4.00

Table 2. Global-averaged results of annual-mean and annual-maximum precipitation trend analysis of the 5 full ISI-MIP climate models from 1951 to 2010. Table shows the results for full land area data of the models, not the subsampled data as shown in Table 1. The 5 ISI-MIP

models give 5 global averages, of which the minimum, maximum, median, mean, and standard deviation are presented.

	Average of precipitation (P) (mm day⁻¹)		Slope of Change (b) (mm day⁻¹ year⁻¹)		Relative change in precipitation (b/ P) (% year⁻¹)		Change per K global warming – Absolute value Average (% K⁻¹)		Change per K global warming – Precipitation weighted Average (% K⁻¹)	
	Mean precip.	Max. precip.	Mean precip.	Max. precip.	Mean precip.	Max. precip.	Mean precip.	Max. precip.	Mean precip.	Max. precip.
ISI-MIP average	2.37	33.43	0.0002	0.0238	0.039	0.074	7.04	12.94	1.74	10.16
ISI-MIP min.	2.34	30.35	-0.0001	0.0081	-0.049	0.014	1.22	4.19	0.61	4.15
ISI-MIP max.	2.40	36.47	0.0007	0.0533	0.089	0.149	15.25	29.64	3.21	20.92
ISI-MIP median	2.39	33.56	0.0000	0.0161	0.072	0.064	8.09	10.77	1.60	7.99
ISI-MIP St.Dev.	0.027	2.928	0.0004	0.0182	0.059	0.055	5.74	10.55	1.02	6.91

Table 3. Global-averaged results of annual-mean and annual-maximum precipitation trend analysis of the 5 ISI-MIP climate models, from 2011 to 2099, under high radiative forcing scenario (RCP8.5). The 5 ISI-MIP models give 5 global averages, of which the minimum, maximum, median, mean, and standard deviation are presented.

	Average of precipitation (P) (mm day^{-1})		Slope of Change (b) (mm day^{-1} year^{-1})		Relative change in precipitation (b/P) (% year^{-1})		Change per K global warming – Absolute value Average (% K^{-1})		Change per K global warming – Precipitation weighted Average (% K^{-1})	
	Mean precip.	Max. precip.	Mean precip.	Max. precip.	Mean precip.	Max. precip.	Mean precip.	Max. precip.	Mean precip.	Max. precip.
ISI-MIP average	2.47	37.77	0.0018	0.0782	0.052	0.165	1.33	3.92	1.61	4.85
ISI-MIP min.	2.39	33.28	0.0005	0.0517	-0.031	0.147	-0.39	2.85	0.33	3.45
ISI-MIP max.	2.51	41.58	0.0030	0.1039	0.110	0.195	2.95	5.03	2.29	7.64
ISI-MIP median	2.49	39.22	0.0021	0.0805	0.057	0.155	1.05	3.63	2.10	4.31
ISI-MIP St.Dev.	0.05	4.05	0.0011	0.0213	0.057	0.021	1.33	0.85	0.86	1.71

Table 4. Global-averaged results of absolute change in decadal volumetric reliability (R_v) of the model RWHS, driven by the 5 subsampled and full ISI-MIP climate models from 1951 to 2010 as well as the ISI-MIP climate models from 2011 to 2099 under high radiative forcing scenario (RCP8.5). Results for the GHCN station observation data are presented as well. The 5 ISI-MIP models give 5 global averages, of which the minimum, maximum, median, mean, and standard deviation are presented.

	Absolute change in decadal R_v (% decade^{-1})						Absolute change in decadal R_v per K global warming (% K^{-1})					
	Sub-Sampled ISI-MIP 1951-2010		Full ISI-MIP 1951-2010		Full ISI-MIP (RCP8.5) 2011-2099		Sub-Sampled ISI-MIP 1951-2010		Full ISI-MIP 1951-2010		Full ISI-MIP (RCP8.5) 2011-2099	
	Real prcp.	Scaled prcp.	Real prcp.	Scaled prcp.	Real prcp.	Scaled prcp.	Real prcp.	Scaled prcp.	Real prcp.	Scaled prcp.	Real prcp.	Scaled prcp.
GHCN	0.199	0.114	-	-	-	-	2.340	1.441	-	-	-	-
ISI-MIP average	-0.151	-0.134	-0.056	-0.072	-0.232	-0.196	-0.600	-0.681	0.233	-0.274	-0.512	-0.412
ISI-MIP min.	-0.341	-0.196	-0.365	-0.208	-0.443	-0.368	-2.148	-1.339	-1.113	-0.802	-1.065	-0.687
ISI-MIP max.	-0.045	-0.094	0.046	0.031	0.010	-0.048	0.360	-0.356	0.763	0.392	0.044	-0.086
ISI-MIP median	-0.139	-0.113	0.030	-0.043	-0.324	-0.199	-0.399	-0.521	0.472	-0.249	-0.587	-0.569
ISI-MIP St.Dev.	0.117	0.046	0.175	0.093	0.194	0.146	0.957	0.390	0.779	0.438	0.471	0.291

Table A1. Minimum necessary tank storage capacity to accommodate a volumetric reliability (R_v) of 95%

		Minimum Tank Storage Capacity (m³) for R_v = 95%						
		50 m²	100 m²	150 m²	200 m²	300 m²	400 m²	600 m²
	0.2 m³	19.75	4.5	3	2.5	2.25	2	1.75
Daily Demand (m³/building)	0.3 m³	infeasible	14	6.75	5	3.75	3.25	2.75
	0.40 m³	infeasible	39.5	14.5	9	6	5	4.5
	0.6 m³	infeasible	infeasible	infeasible	28	13.5	10	7.5

Figure Captions

Figure 1. A behavioral model configuration for a RWHS

Figure 2. GHCN observational data results for mean and maximum precipitation for 1951-2010: Annual-average daily precipitation (mean precipitation) map (mm day^{-1}) (a), Annual-maximum daily precipitation (maximum precipitation) map (mm day^{-1}) (d), Relative change in annual-average daily precipitation (mean precipitation) map (% year^{-1}) map (b), Relative change in annual- maximum daily precipitation (maximum precipitation) map (% year^{-1}) map (e), Relative change in mean precipitation per K of global warming (% K^{-1}) map (c) and Relative change in maximum precipitation per K of global warming (% K^{-1}) map (f).

Figure 3. Box plots of full and sub-sampled ISI-MIP climate model runs averaged results (minimum, 25th percentile, median, 75th percentile and maximum of the 5 model runs) as well as average of GHCN observational data (shown as colored circles) for 1951–2010 and 2011-2099 (RCP8.5) precipitation data at global and continental scales. Panels a-c show box plots of relative change in mean and maximum precipitation (% year^{-1}) for Sub-Sampled ISI-MIP 1951-2010, full ISI-MIP 1951-2010 and full ISI-MIP 2011-2099, respectively. Panels d-f are box plots of relative change in mean and maximum precipitation per K of global warming (% K^{-1}) for Sub-Sampled ISI-MIP 1951-2010, full ISI-MIP 1951-2010 and full ISI-MIP 2011-2099, respectively. The yellow colored boxes represent the results of mean precipitation and the un-shaded boxes represent the maximum precipitation for the models. The blue and purple circles in (a) and (d) represent the GHCN average results for mean and maximum precipitation, respectively. The red plus-shaped markers shown outside some of the boxes represent model outliers.

Figure 4. Boxplots of ISI-MIP model runs averaged reliability trends (minimum, 25th percentile, median, 75th percentile and maximum of the 5 model runs) as well as average of GHCN observational data (shown as colored circles) for 1951–2010 and 2011-2099 precipitation data in global and continental scale. (a), (b) and (c) represent the boxplots of change in decadal volumetric reliability (R_v) of the RWHS system (% decade[-1]) for real and scaled precipitation for full ISI-MIP 1951-2010, Sub-Sampled ISI-MIP 1951-2010 and full ISI-MIP 2011-2099, respectively. (d), (e) and (f) represent the boxplots of change in decadal volumetric reliability (R_v) of the RWHS system per K of global warming (% K[-1]) for full ISI-MIP 1951-2010, Sub-Sampled ISI-MIP 1951-2010 and full ISI-MIP 2011-2099, respectively. The yellow-shaded boxes represent the results of mean precipitation and the un-shaded boxes represent the maximum precipitation from the models. The green and purple circles represent the GHCN average for mean and maximum precipitation, respectively. The few red plus-shaped markers shown outside some of the boxes represent model outliers.

Figure 5. Global maps of change in decadal volumetric reliability (R_v) of the RWHS system driven by GHCN station observation data for 1951-2010: (a) and (b) represent the relative change R_v (% decade[-1]) for actual and scaled precipitation, respectively. (c) and (d) represent the relative in R_v per K of global warming (% K[-1]) for actual and scaled precipitation, respectively.
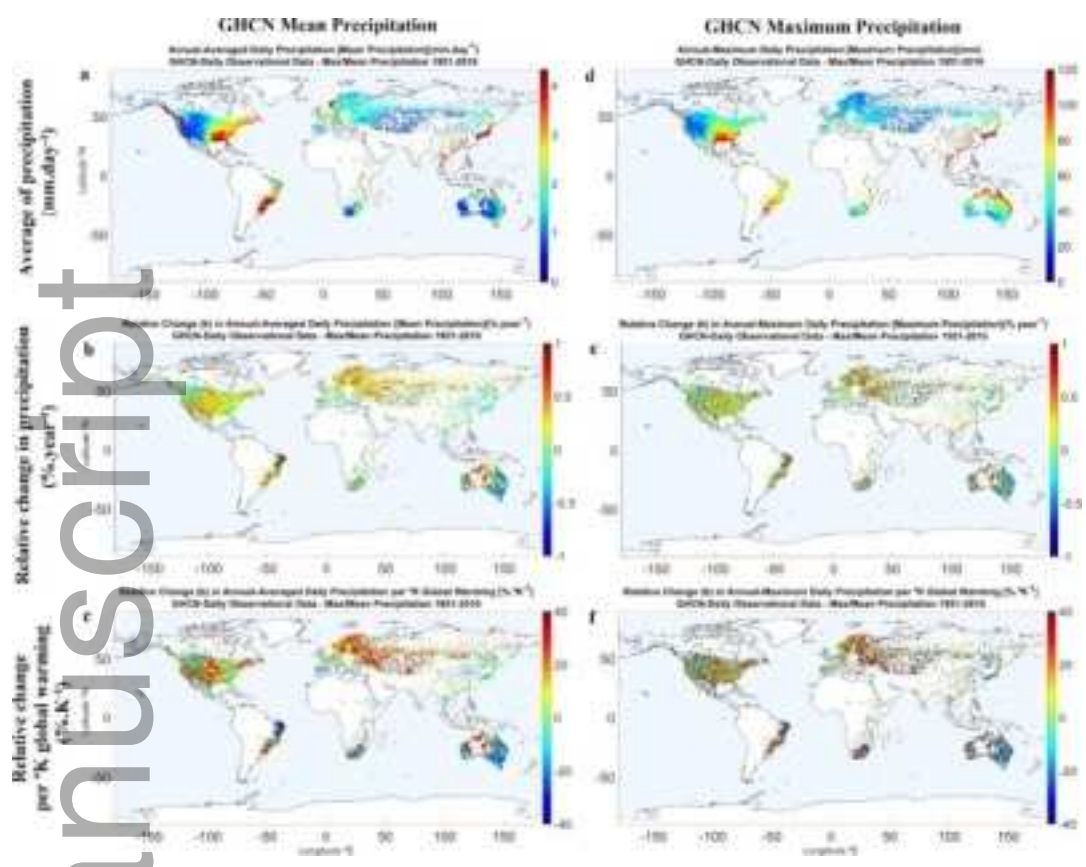
Figure 6. Plots of global-averaged results for different precipitation deciles, with lower percentiles representing the driest areas and higher deciles representing the wettest areas: Relative change in precipitation (% decade[-1]) for full land area data from ISI-MIP models for 1951-2010 (a) and 2011-2099 (RCP8.5) (c), absolute change in decadal volumetric reliability (R_v) of the model RHWS driven by full ISI-MIP dataset for 1951-2010 (b) and 2011-2099 (RCP8.5) (d). Plots show average of the 5 models.

Figure 7. Plots of global-averaged results for different precipitation deciles, with lower percentiles representing the driest areas and higher deciles representing the wettest areas: Relative change in precipitation (% decade[-1]) for GHCN station observations (a) and the 5 subsampled ISI-MIP models (c) for 1951-2010, absolute change in decadal volumetric reliability (R_v) of the model RHWS driven by GHCN station observations (b) and the 5 subsampled ISI-MIP models (d) for 1951-2010. For the ISI-MIP results, plots show average of the 5 models.
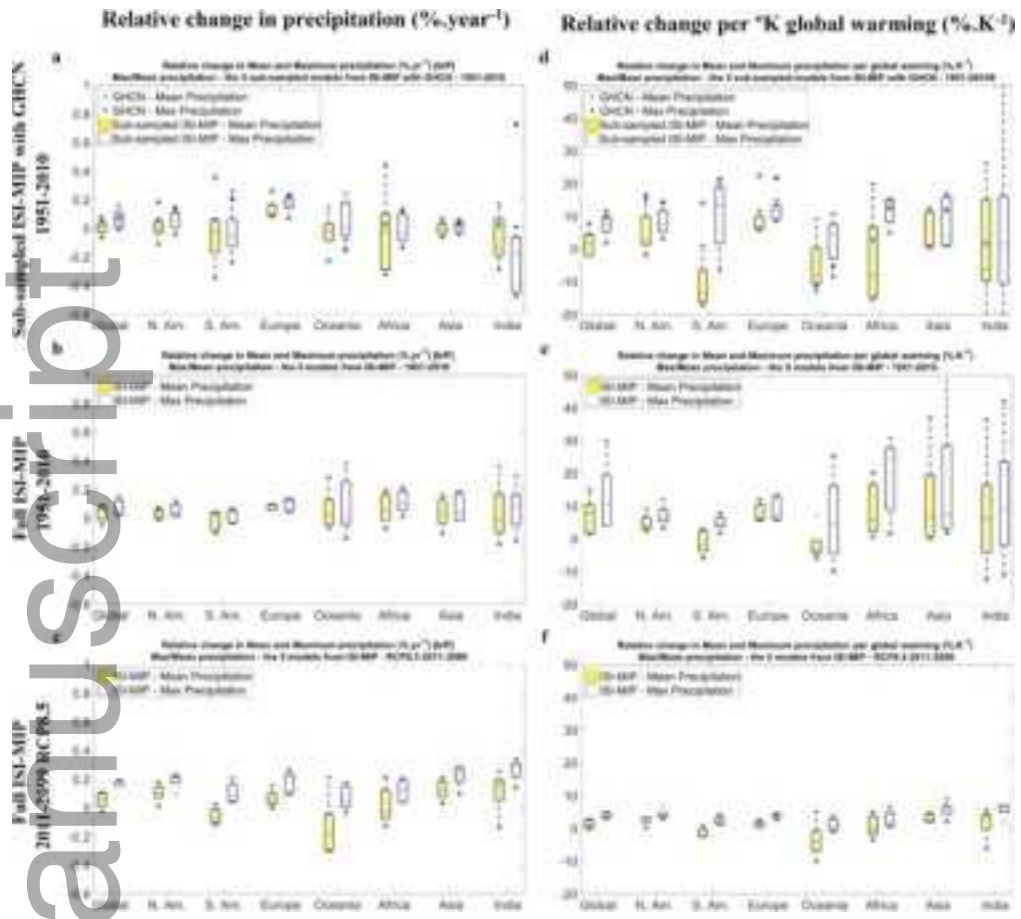
Figure A1. a) Volumetric reliability (R_v) of the model rainwater harvesting system vs. storage capacity at various catchment area for daily demands of 0.2 and 0.4 m[3]. b) Volumetric reliability of the system vs. specific storage capacity (day) at various specific catchment area values.
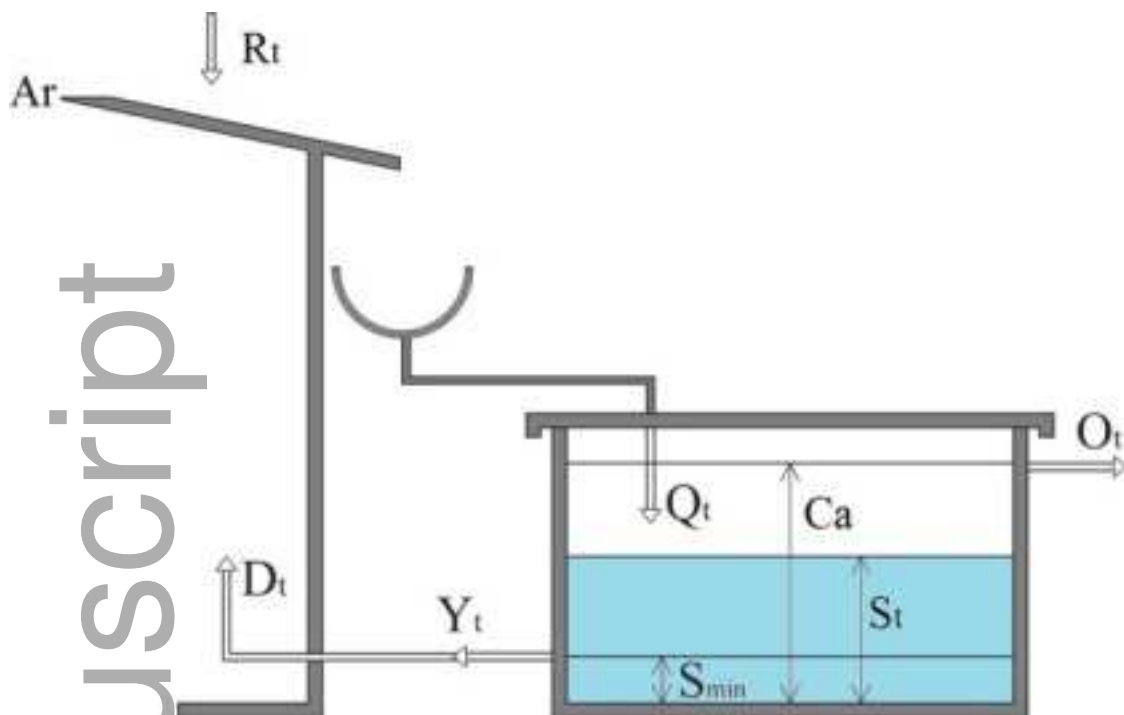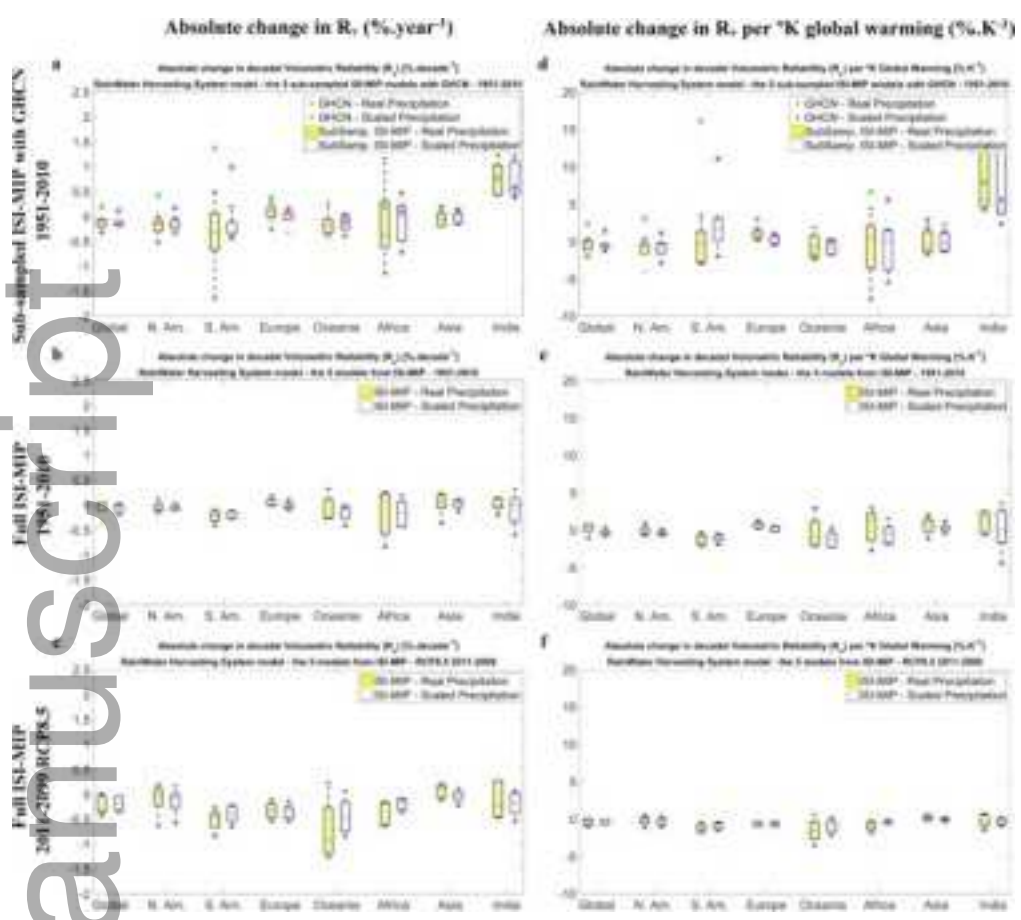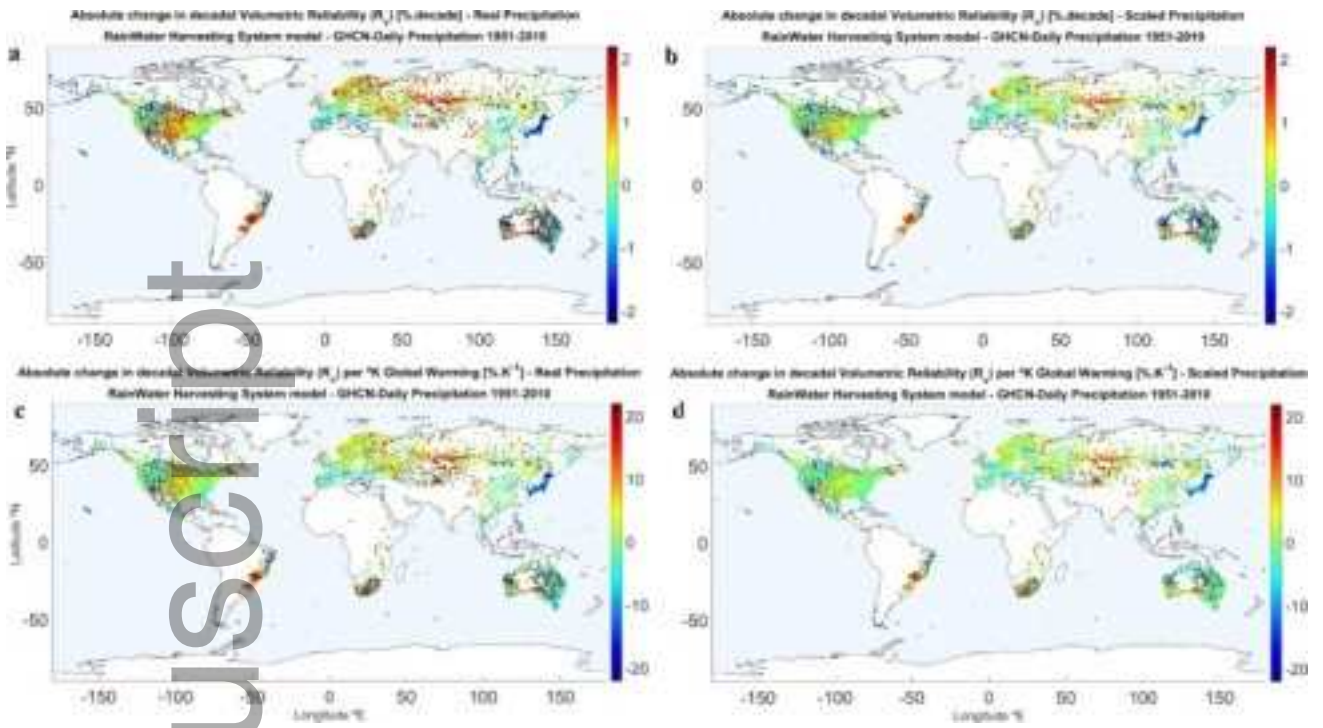
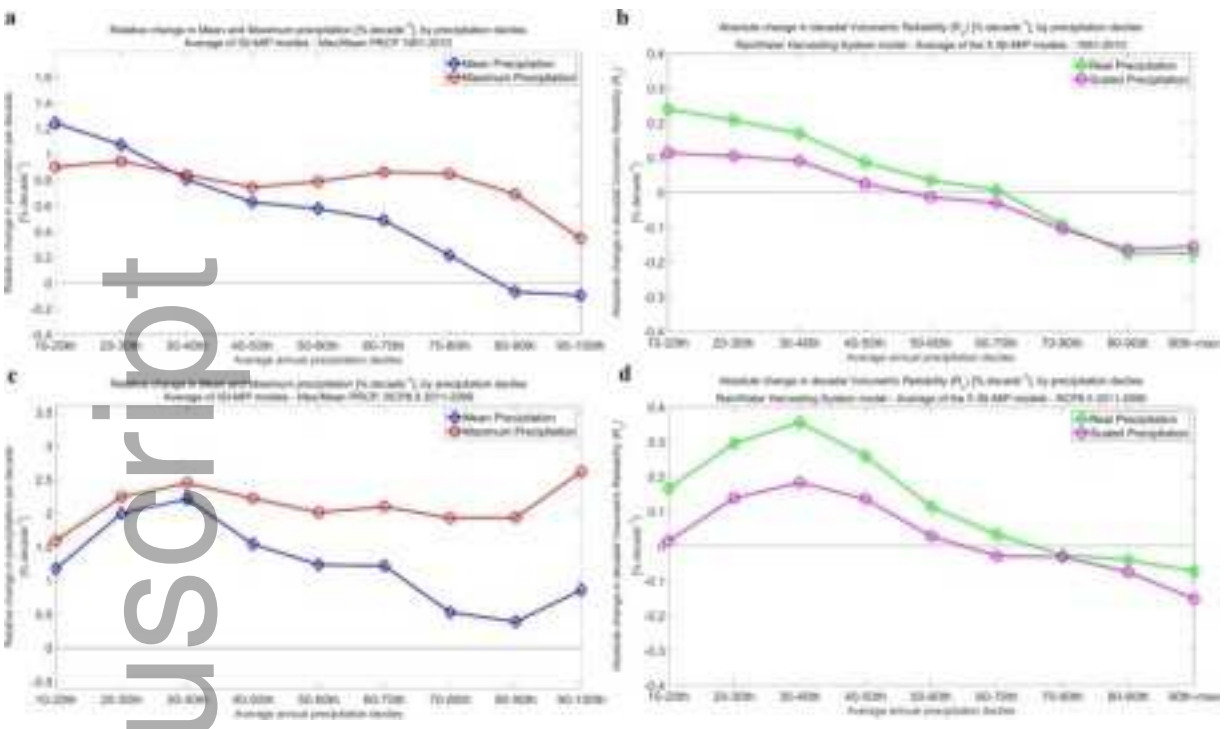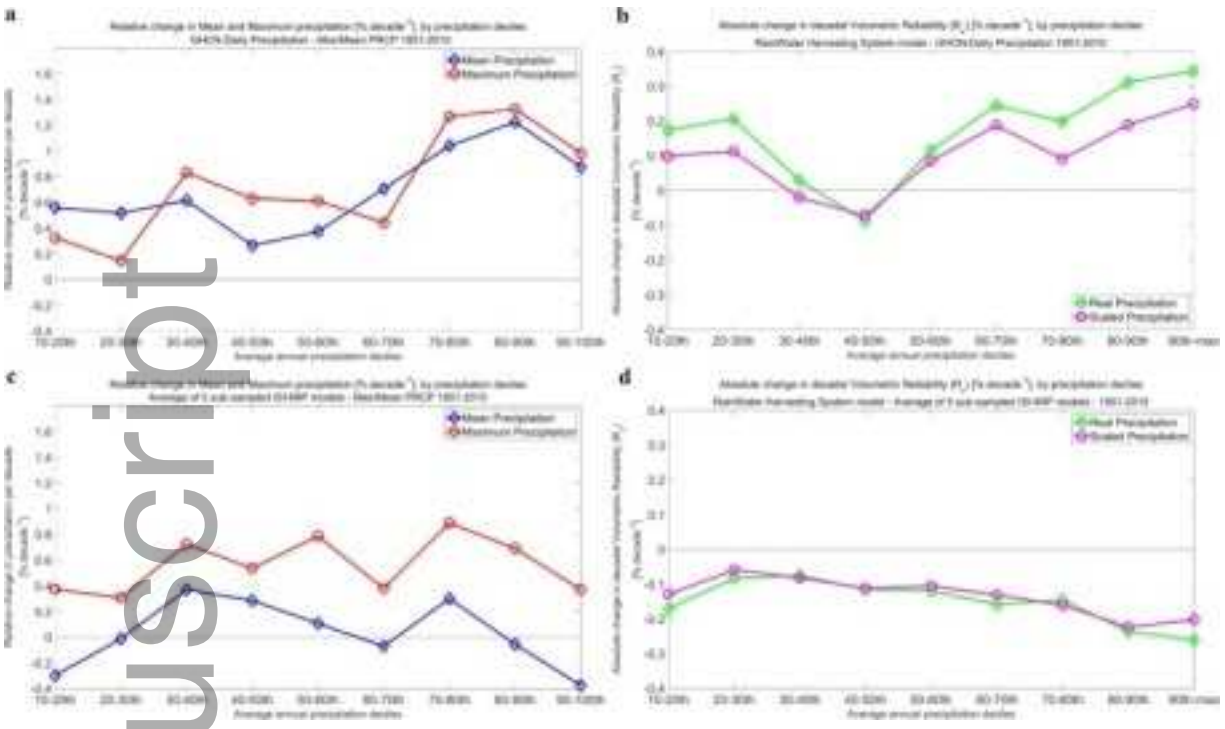jawra_12472-15-0179_f1.tif

jawra_12472-15-0179_f2.tif

jawra_12472-15-0179_f3.tif

jawra_12472-15-0179_f4.tif

Absolute change in decadal Volumetric Reliability (R_v) [%/decade] - Real Precipitation
RainWater Harvesting System model - GHCN-Daily Precipitation 1951-2010

Absolute change in decadal Volumetric Reliability (R_v) [%/decade] - Scaled Precipitation
RainWater Harvesting System model - GHCN-Daily Precipitation 1951-2010

Absolute change in decadal Volumetric Reliability (R_v) per °K Global Warming [%.K⁻¹] - Real Precipitation
RainWater Harvesting System model - GHCN-Daily Precipitation 1951-2010

Absolute change in decadal Volumetric Reliability (R_v) per °K Global Warming [%.K⁻¹] - Scaled Precipitation
RainWater Harvesting System model - GHCN-Daily Precipitation 1951-2010

jawra_12472-15-0179_f5.tif

jawra_12472-15-0179_f6.tif

jawra_12472-15-0179_f7.tif